

Supplementary Information

The favorable thermodynamic properties of Fe-doped CaMnO₃ for thermochemical heat storage

Emanuela Mastronardo^{1,2, a)}, Xin Qian², Juan M. Coronado¹ and Sossina M. Haile^{2, b)}

¹ Institute of Catalysis and Petrochemistry, Spanish National Research Council (CSIC), C/ Marie Curie, 2. E-28049. Madrid, Spain.

² Materials Science and Engineering, Northwestern University, 2220 Campus Drive Cook Hall, 60208 Evanston, IL, United States.

Corresponding authors: ^{a)}e.mastronardo@csic.es
^{b)}sossina.haile@northwestern.edu

Appendix A

A.1 Initial oxygen non-stoichiometry (δ_0) measurement

The initial oxygen non-stoichiometry was evaluated through complete reduction of the material at 1000 °C under 3% H₂/Ar flow with TGA measurement (Figure A 1a). In case of CMF73, the residual composition has been analyzed by XRD (Figure A 1b). In case of the un-doped CM, after complete reduction the product is Ca_{0.5}Mn_{0.5}O. While, in case of the Fe-doped CM, it was detected the presence of metallic Fe and of Mn_{0.18}Fe_{0.82} together with a composition of Ca_xMn_{1-x}O (Ca_{0.53}Mn_{0.47}O and Ca_{0.6}Mn_{0.4}O, respectively for CMF91 and CMF73) that can be indexed as Ca_{0.5}Mn_{0.5}O phase.

Considering the following reaction stoichiometry for the samples decompositions:



from the oxygen balance equations, the initial oxygen non-stoichiometry (δ_0) has been estimated to be 0.0017, 0.043, and 0.1538 respectively for CM, CMF91 and CMF73.

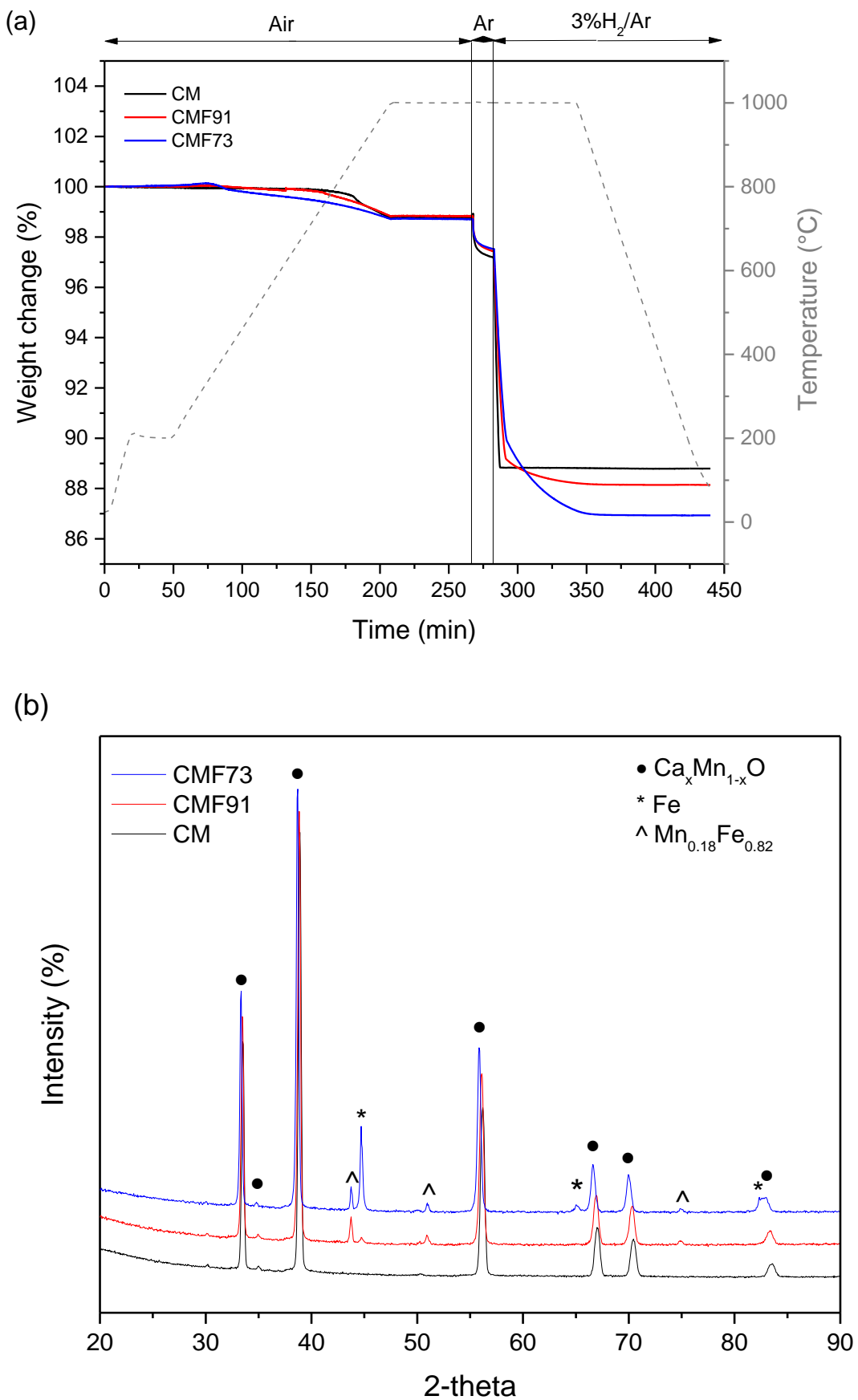


Figure A 1. (a) TGA analysis under 3% H₂/Ar. (b) XRD patterns after TGA analysis.

A.2 SEM/EDX analysis

Macro- and meso-porosities are observable from SEM micrographs (see Figure A 2) on sintered samples' monoliths, this allows the gas flowing through the samples during the analysis. No impurities were detected through EDX analysis (see Figure A 3). EDX detected Ca and Mn in case of CM, and Ca, Mn and Fe in case of CMF91 and CMF73 samples. Ca and Mn K α mapping are reported for completeness in Figure A 4.

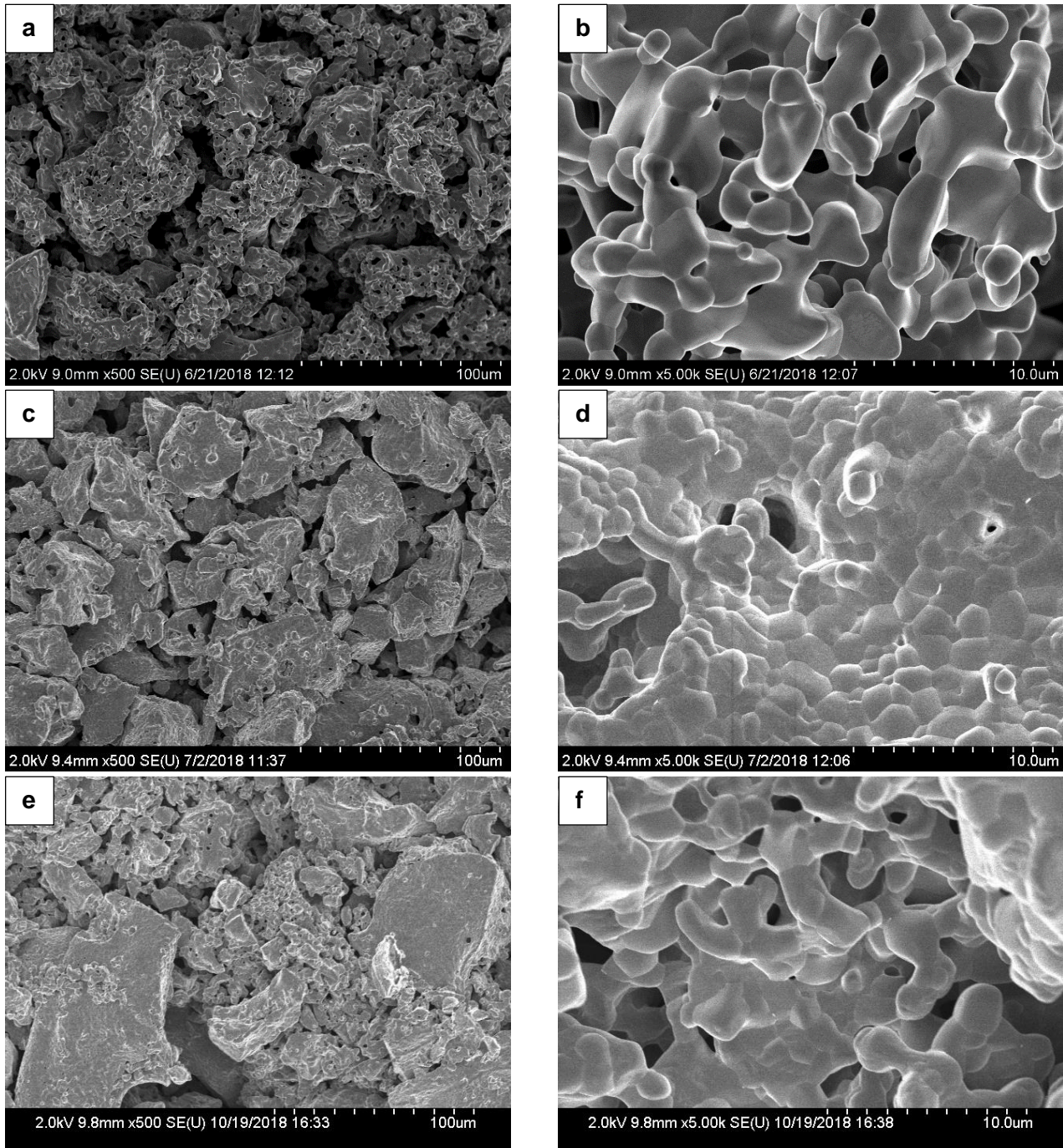


Figure A 2. SEM micrographs of (a, b) CM, (c, d) CMF91, (e, f) CMF73 samples.

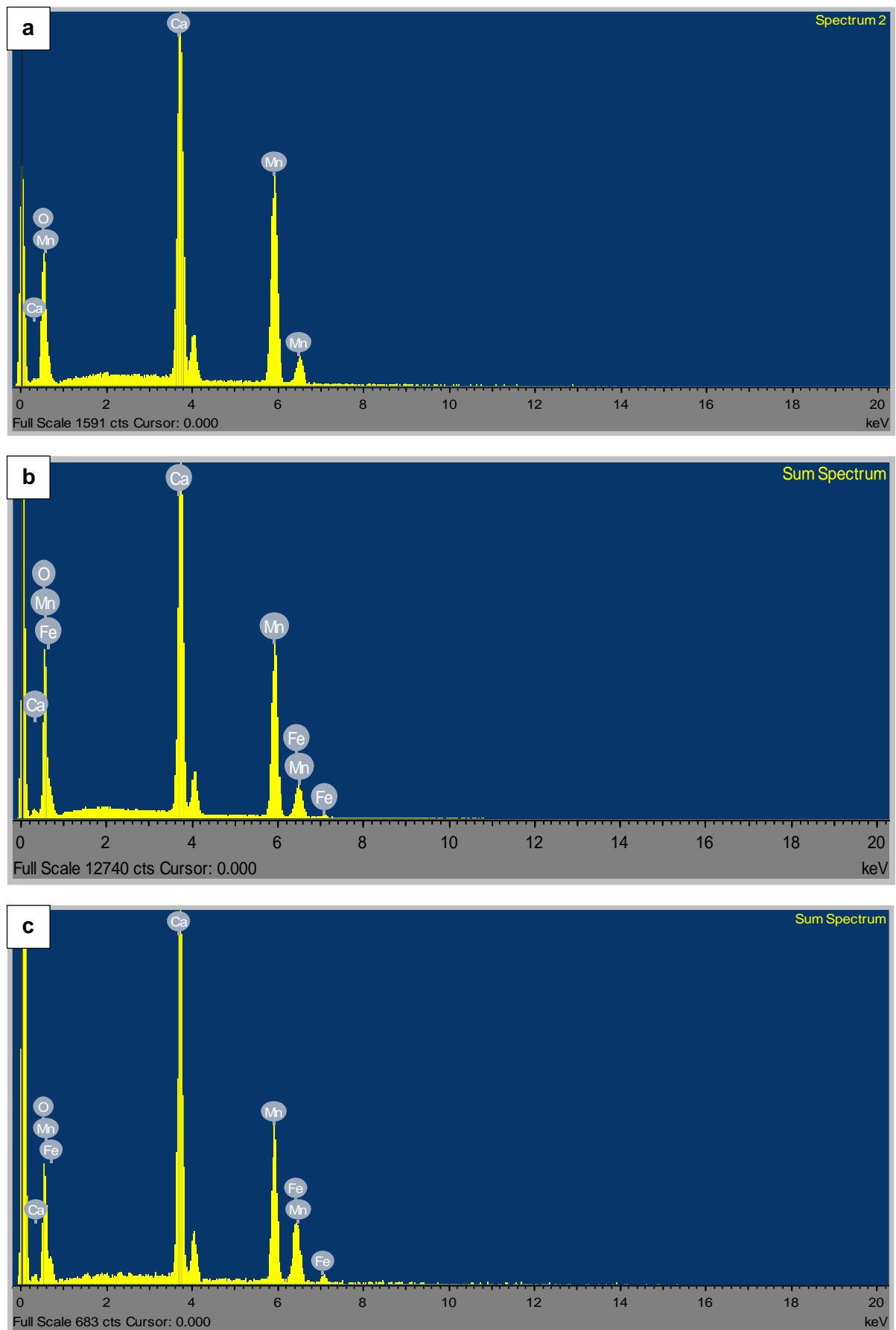


Figure A 3. EDS spectra of (a) CM, (b) CMF91 and (c) CMF73 samples.

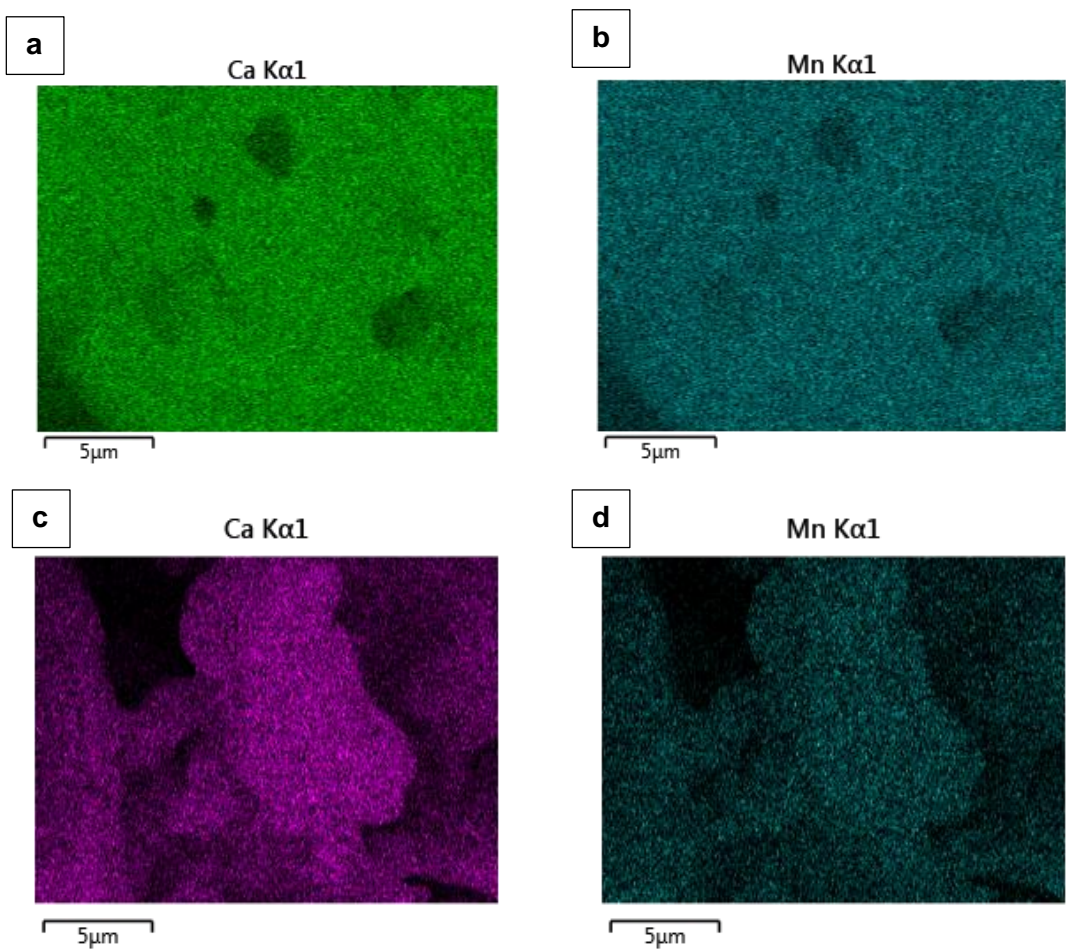


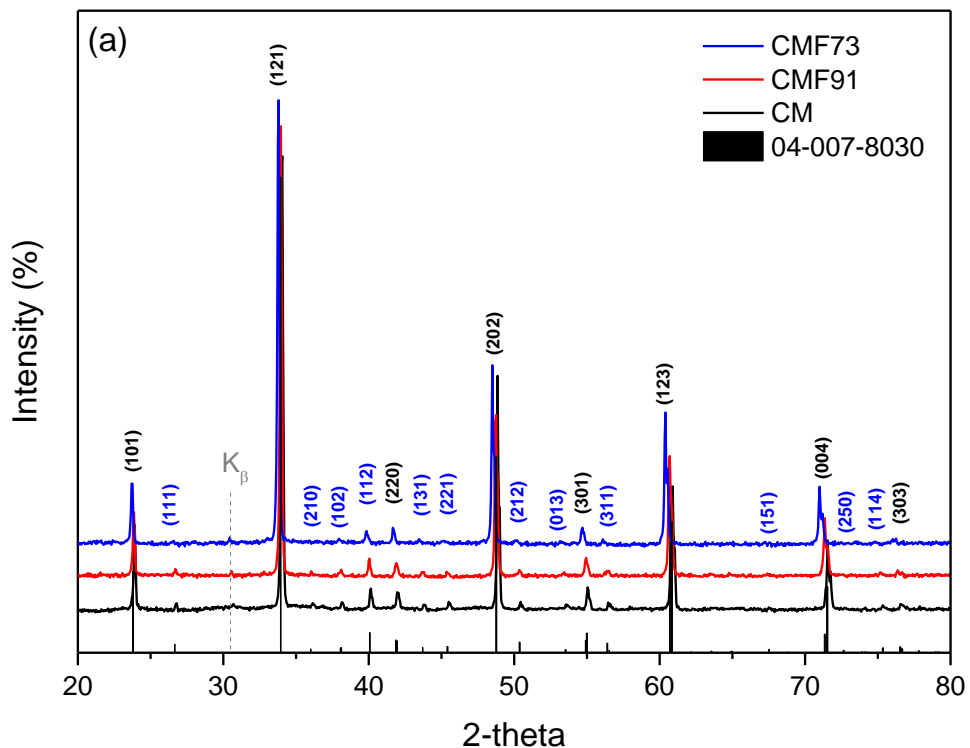
Figure A 4. Ca and Mn K α 1 mapping on (a,b) CMF91 and (c,d) CMF73 samples.

A.3 XRD analysis of as synthesized samples

XRD analysis of the as prepared materials are reported in Figure A 5a, with the detail of the most intense peaks (Figure A 5b). The theoretical density, computed by Rietveld refinement and used for the conversion of the heat storage capacity from mass to volume unit, is listed in the following Table.

Table A.3.1. Computed theoretical density by Rietveld refinement.

Code	ρ (kg/m ³)
CM	4820
CMF91	4814
CMF73	4834



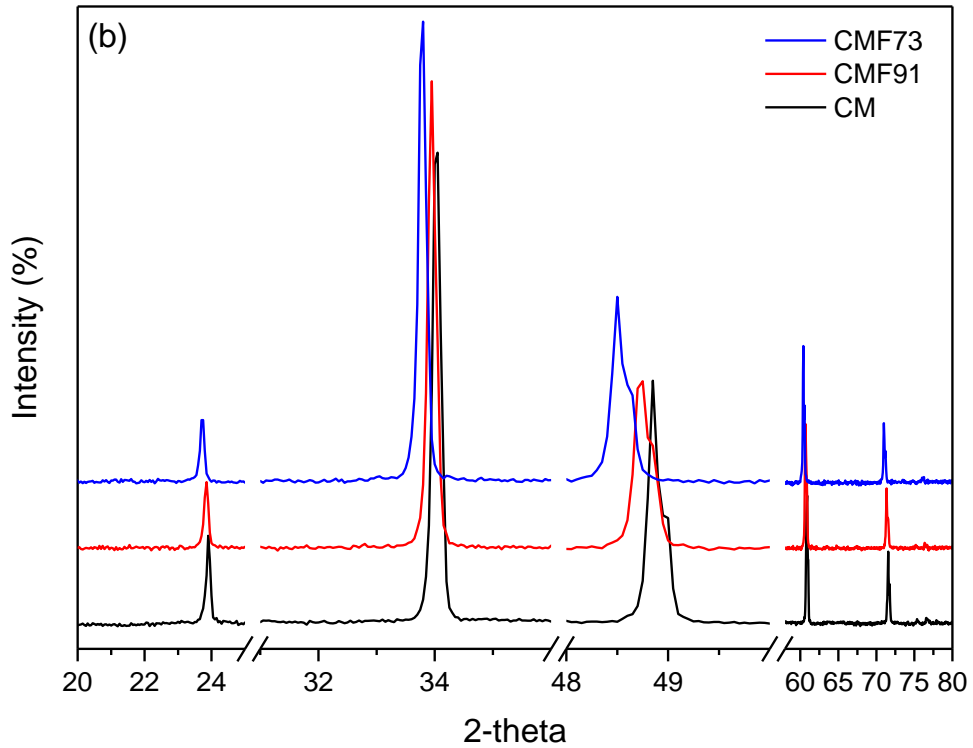


Figure A 5. (a) XRD pattern of un-doped and Fe-doped CaMnO₃. (b) Detail of the most intense peaks.

A.4 TG/DSC additional data

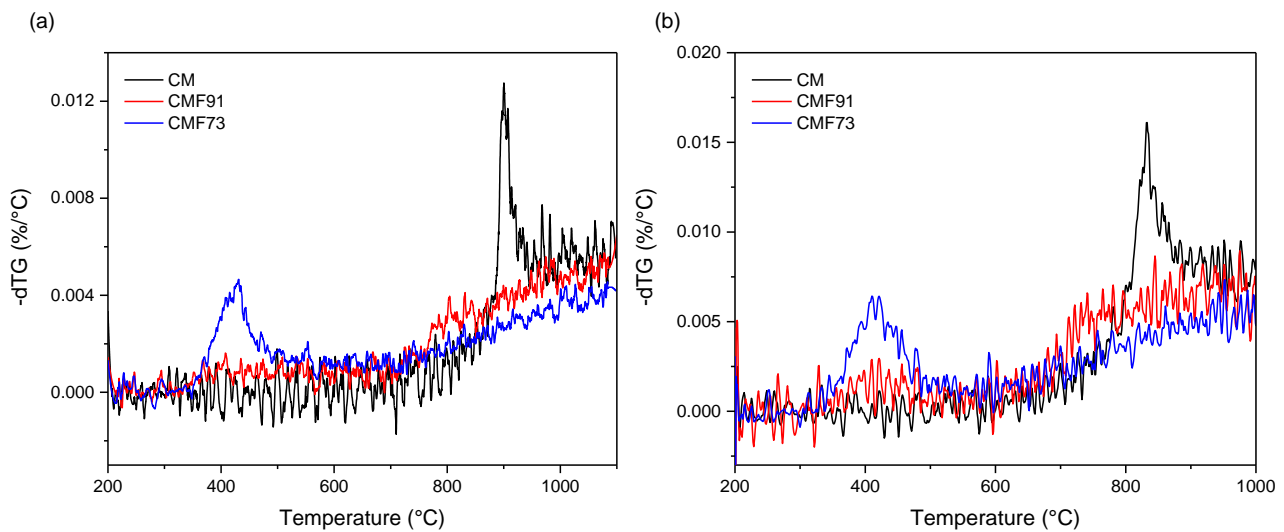


Figure A.6. Differential mass loss curves of CM, CMF91 and CMF73 on (a) heating to 1100 °C at a ramp rate of 10 °C/min under a pO_2 of 0.18 atm and on (b) heating to 1000 °C at a ramp rate of 10 °C/min under a pO_2 of 5.1×10^{-4} atm.

The enthalpy values relative to the phase change from the orthorhombic to cubic structure are reported in the following Table:

Table A.4.1. Phase change enthalpy values measured from DSC signals.

Code	$pO_2=0.18$ atm					$pO_2 5 \cdot 10^{-4}$ atm			
	1 st peak		2 nd peak		ΔH (kJ/kg _{ABO₃})	$\Delta\delta$	ΔH (kJ/molo)	1 st peak	
	T _{peak} (°C)	T _{peak} (°C)	ΔH (kJ/kg _{ABO₃})	$\Delta\delta$				T _{peak} (°C)	ΔH (kJ/kg _{ABO₃})
CM	894.3	913.2	36.4 (total)	0.033	157.6			829.8	24.1
CMF91	794.0	-	17.6	0.042	79.1			736.4	24.7
CMF73	433.1	-	13.6	0.028	69.5			421.8	20.2

A.5 Lattice parameters evolution as a function of temperature

The refined lattice parameters of CM, CMF91 and CMF73 for each temperature scan are listed in the following Tables:

Table A.5.1. Refined lattice parameters of CM for each temperature scan.

Temperature (°C)	Phase Identified	Structure	Space Group	Lattice parameters		
				a (Å)	b (Å)	c (Å)
r.t.	CaMnO ₃	Orthorhombic	Pnma	5.2785 (4)	7.4564 (5)	5.2664 (2)
300	CaMnO ₃	Orthorhombic	Pnma	5.2912 (1)	7.4830 (1)	5.2866 (4)
350	CaMnO ₃	Orthorhombic	Pnma	5.2930 (9)	7.4882 (1)	5.2900 (3)
400	CaMnO ₃	Orthorhombic	Pnma	5.2954 (3)	7.4931 (0)	5.2937 (4)
450	CaMnO ₃	Orthorhombic	Pnma	5.2989 (0)	7.4969 (0)	5.2963 (5)
550	CaMnO ₃	Orthorhombic	Pnma	5.3048 (1)	7.5076 (7)	5.3033 (2)
700	CaMnO ₃	Orthorhombic	Pnma	5.3134 (5)	7.5249 (1)	5.3171 (3)
800	CaMnO ₃	orthorhombic; cubic	Pnma;	5.3209 (1);	7.5379 (0);	5.3273 (4);
1000	CaMnO ₃	Cubic	Pm-3m	3.7662 (1)	3.7662 (1)	3.7662 (1)
1100	CaMnO ₃ ; Ca ₂ MnO ₄ ; CaMn ₂ O ₄	-	Pm-3m	3.7859 (1)	3.7859 (1)	3.7859 (1)

Table A.5.2. Refined lattice parameters of CMF91 for each temperature scan.

Temperature (°C)	Phase Identified	Structure	Space Group	Lattice parameters		
				a (Å)	b (Å)	c (Å)
r.t.	CaMnO ₃	orthorhombic	Pnma	5.2906 (5)	7.4737 (4)	5.2804 (7)
300	CaMnO ₃	orthorhombic	Pnma	5.3032 (3)	7.5044 (7)	5.2971 (8)
350	CaMnO ₃	orthorhombic	Pnma	5.3057 (8)	7.5095 (8)	5.3012 (9)
400	CaMnO ₃	orthorhombic	Pnma	5.3092 (4)	7.5152 (5)	5.3045 (2)
450	CaMnO ₃	orthorhombic	Pnma	5.3126 (8)	7.5212 (5)	5.3083 (0)
550	CaMnO ₃	orthorhombic	Pnma	5.3210 (1)	7.5308 (11)	5.3144 (1)
700	CaMnO ₃	orthorhombic; cubic	Pnma;	5.3359 (0);	7.5469 (12);	5.3262 (4);
800	CaMnO ₃	cubic	Pm-3m	3.7717 (8)	3.7717 (8)	3.7717 (8)
1000	CaMnO ₃	cubic	Pm-3m	3.7954 (5)	3.7954 (5)	3.7954 (5)
1100	CaMnO ₃	cubic	Pm-3m	3.8011 (3)	3.8011 (3)	3.8011 (3)

Table A.5.3. Refined lattice parameters of CMF73 for each temperature scan.

Temperature (°C)	Phase Identified	Structure	Space Group	Lattice parameters		
				a (Å)	b (Å)	c (Å)
r.t.	CaMnO ₃	orthorhombic	Pnma	5.3093 (8)	7.5102 (5)	5.3054 (9)
300	CaMnO ₃	orthorhombic	Pnma	5.3253 (4)	7.5237 (9)	5.3210 (1)
350	CaMnO ₃	orthorhombic;	Pnma;	5.3309 (11);	7.5288 (9);	5.3242 (1);
		cubic	Pm-3m	3.7655 (6)	3.7655 (6)	3.7655 (6)
400	CaMnO ₃	orthorhombic;	Pnma;	5.3353 (6);	7.5350 (2);	5.3278 (0);
		cubic	Pm-3m	3.7691 (3)	3.7691 (3)	3.7691 (3)
450	CaMnO ₃	cubic	Pm-3m	3.7738 (7)	3.7738 (7)	3.7738 (7)
550	CaMnO ₃	cubic	Pm-3m	3.7801 (2)	3.7801 (2)	3.7801 (2)
700	CaMnO ₃	cubic	Pm-3m	3.7880 (2)	3.7880 (2)	3.7880 (2)
800	CaMnO ₃	cubic	Pm-3m	3.7955 (7)	3.7955 (7)	3.7955 (7)
1000	CaMnO ₃	cubic	Pm-3m	3.8147 (8)	3.8147 (8)	3.8147 (8)
1100	CaMnO ₃	cubic	Pm-3m	3.8253 (4)	3.8253 (4)	3.8253 (4)

A.6 Samples pO₂(T) profiles and weights

As it can be observed from Figure A 7, the oxygen sensor recorded for all the samples small variations of pO₂ value over the course of the experiment with the exception of phase change events.

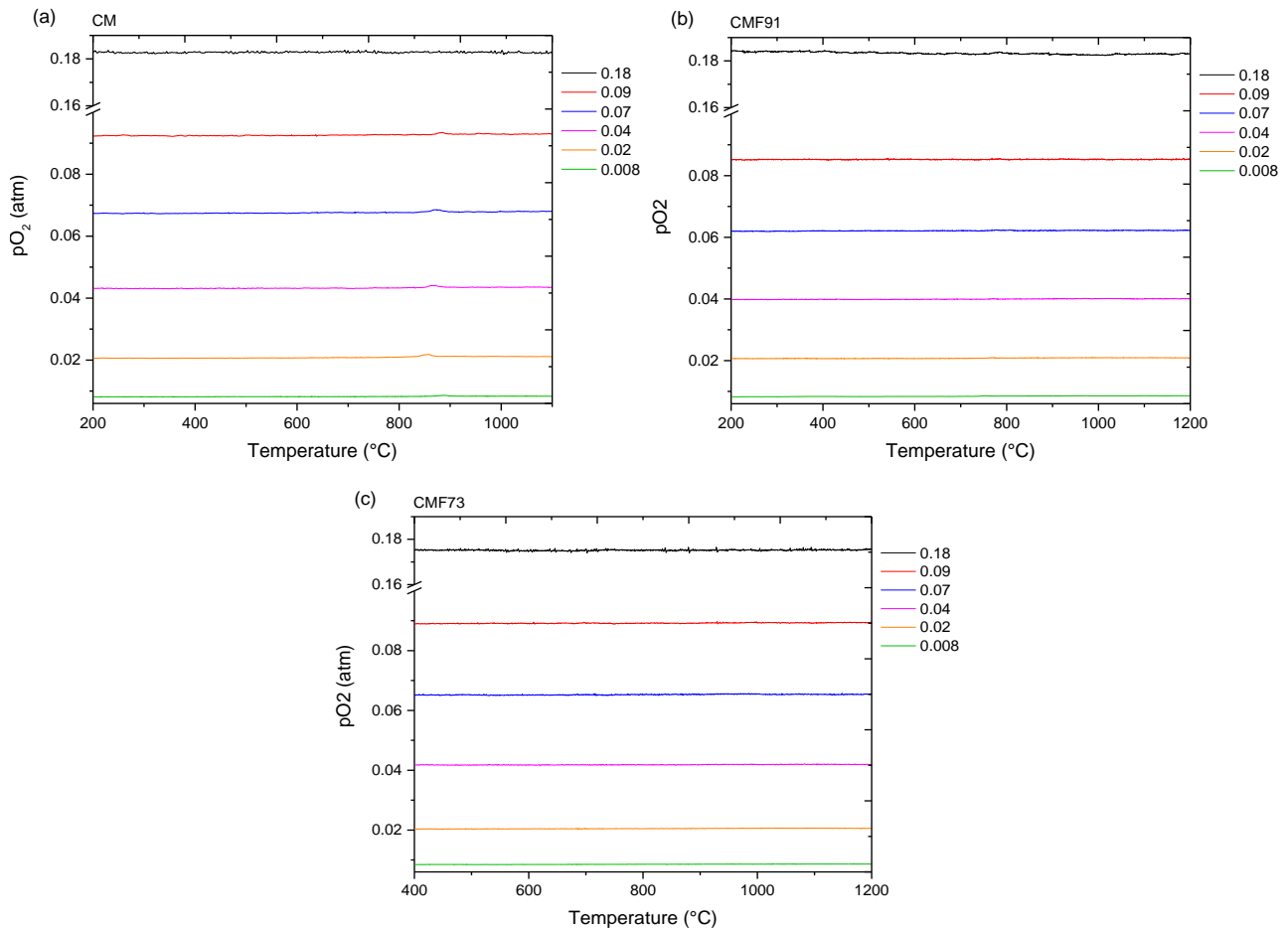


Figure A 7. $pO_2(T)$ profiles of (a) CM, (b) CMF91 and (c) CMF73 samples.

In Figure A 8 is shown an example of monolith used for TG analysis. About 20 kgf hav been applied for pressing the pellet.



Figure A 8. Example of monolith used for TGA.

Table A.6.1. Weight of the samples' pellet used for TGA measurements for thermodynamic data extraction.

pO₂ (atm)	TGA Samples weight (mg)		
	CM	CMF91	CMF73
0.18	519.48	407.35	271.89
0.09	476.02	407.05	271.81
0.07	526.04	407.31	270.93
0.04	525.92	407.25	270.88
0.02	271.43	407.31	270.72
0.008	211.70	407.00	271.37

A.7 XRD analysis after TG/DSC measurements

In Figure A 9 are shown the XRD pattern of the samples after the TG measurements. The CMF73 material was found to be a mixture of cubic and orthorhombic phases after cooling under 0.008 atm from 1200 °C. It is unclear whether the equilibrium state at ambient temperature and low oxygen partial pressure is a mixture of these two phases (obtained on cooling) or only the orthorhombic phase (obtained after the initial equilibration at 200 °C at the onset of the experiment).

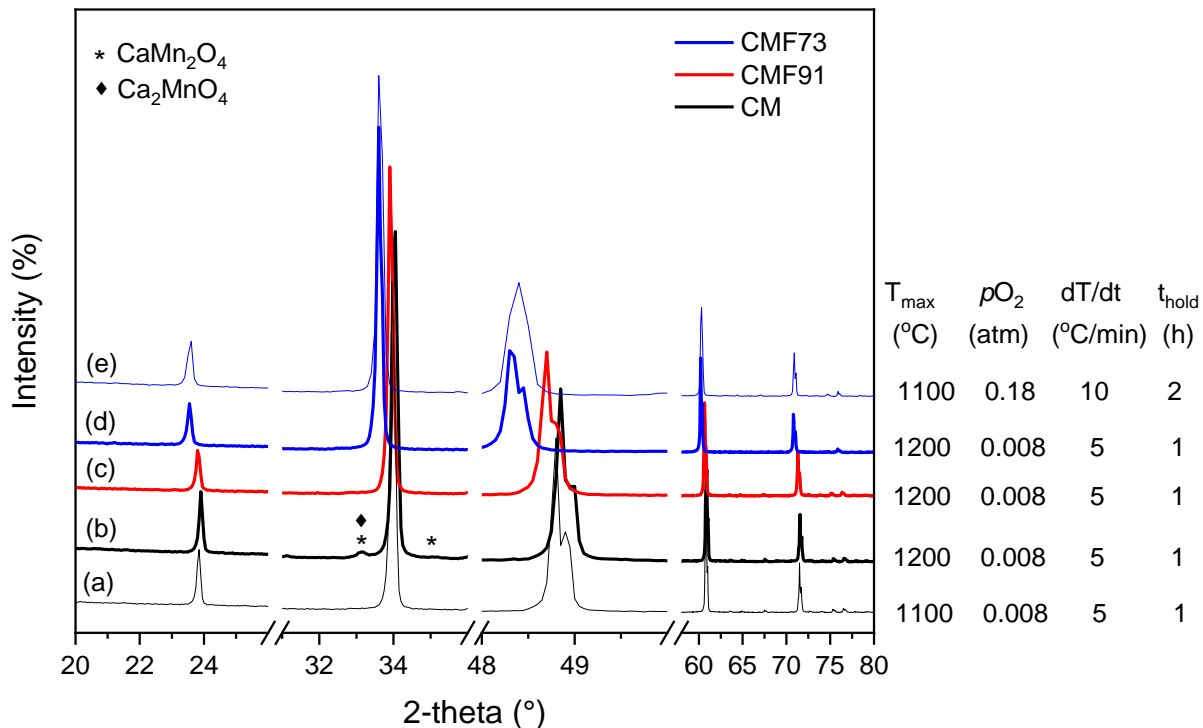


Figure A 9. XRD patterns of CM and CMF materials after TGA measurement under the conditions indicated. Patterns (a), (c) and (d) correspond to the most reducing condition used for the thermodynamic data extraction. The patterns are collected after 2-12 h after completion of the TGA experiments.

Table A.7. 1. Lattice parameters of Fe-doped CaMnO_3 corresponding to patterns shown in Figure A.9 Volume increase relative to the as-synthesized condition is also reported.

Code	Pattern	Phase type	Amount (wt.%)	Lattice parameters				
				V_{cell} (Å ³)	V_{increase} (%)	a (Å)	b (Å)	c (Å)
CM*	(b)	orthorhombic	92	207.48 (2)	0.10 (1)	5.2817 (2)	7.4580 (4)	5.2671 (2)
CMF91	(c)	orthorhombic	100	208.90 (9)	0.06 (1)	5.2920 (1)	7.4744 (2)	5.2814 (1)
CMF73	(d)	orthorhombic	68	211.72 (6)	0.09 (2)	5.3125 (7)	7.5075 (2)	5.3084 (1)
		cubic	32	59.92 (3)	-	3.7544 (7)	3.7544 (7)	3.7544 (7)
CMF73	(e)	orthorhombic	100	211.88 (4)	0.16 (2)	5.3119 (1)	7.5140 (2)	5.3086 (7)

*as measured in the presence of minor impurity phases: Ca_2MnO_4 and CaMn_2O_4 .

A.8 Arrhenius plot

In Figure A 10 are shown the Arrhenius plots of (a) CMF91 and (b) CMF73 used to extract thermodynamic parameters for the cubic and orthorhombic phases, over the respective T- $p\text{O}_2$ ranges. Reported in Table A.8 .1 are the effective enthalpy and entropy values defining the phase boundaries in the CM and CMF91 systems.

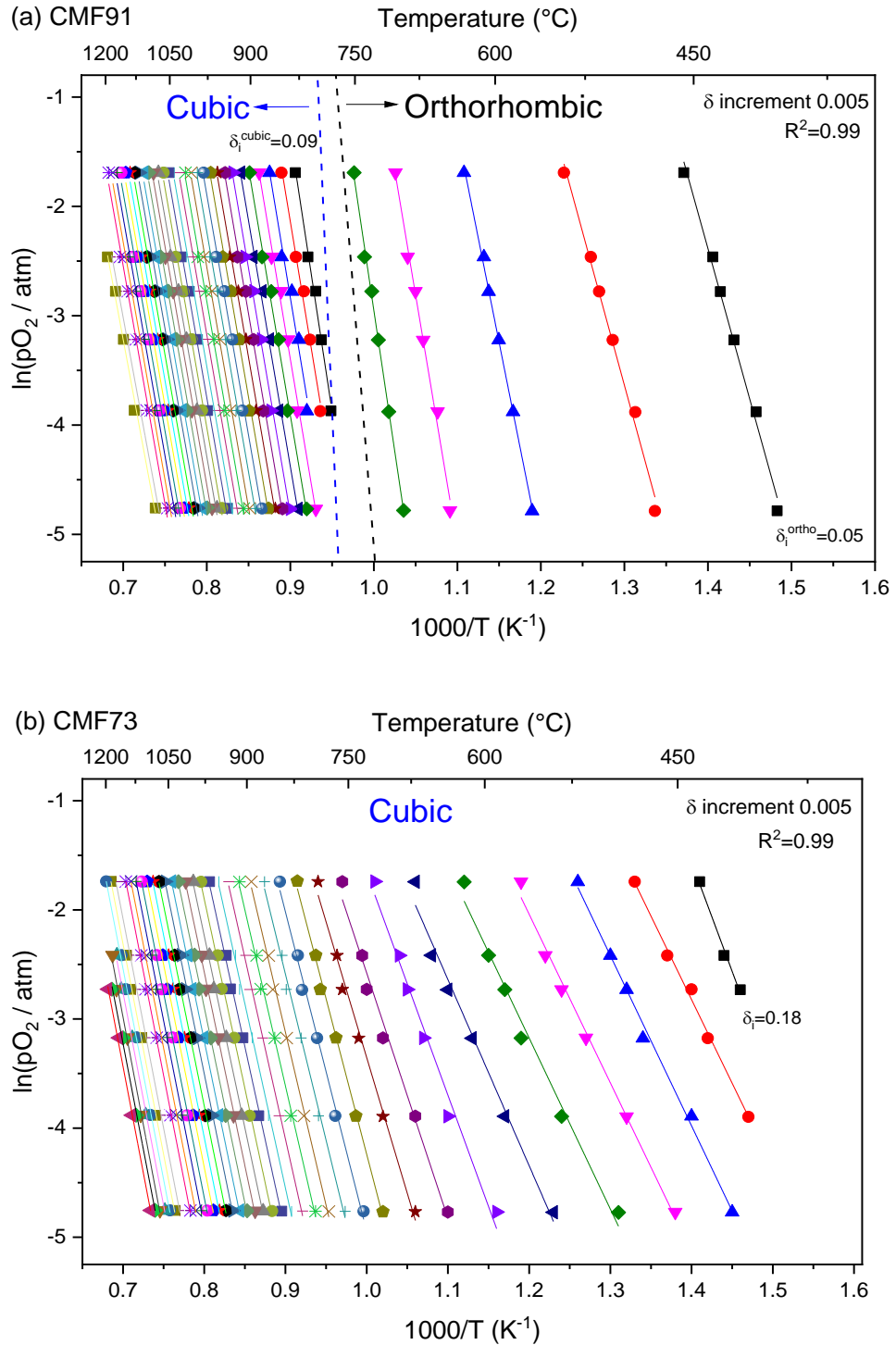


Figure A 10. Arrhenius plot of (a) CMF91 and (b) CMF73 used to extract thermodynamic parameters for the cubic and orthorhombic phases, over the respective T- $p\text{O}_2$ ranges shown.

Table A.8. 1. Enthalpy and entropy values defining the phase boundaries in the CM and CMF91 systems.

CM	Δho (kJ/molo)	Δso (J/K·molo)
Phase transition	CM	CM
T _{onset} (O→T)	246.13 ± 8.91	207.79 ± 7.99
T _{onset} (T→C)	316.07 ± 18.08	261.71 ± 15.56
T _{end} (T→C)	287.22 ± 9.36	234.07 ± 8.05

CMF91	Δho (kJ/molo)	Δso (J/K·molo)
Phase transition	CMF91	CMF91
T _{onset} (O→C)	394.57 ± 19.68	373.30 ± 19.27
T _{end} (O→C)	736.40 ± 23.39	683.47 ± 22.13

A.9 Molar entropy

The extracted molar entropy (Δs_o (J/mol_O·K)) for the undoped and Fe-doped CM is shown in Figure A 11. In the orthorhombic regime, similarly to the molar enthalpy, the extracted entropy is a function of δ for each sample, whereas in the cubic regime it is almost constant for CM and CMF91. For CMF73, the entropy in cubic regime increases in the δ range between 0.19-0.23 approaching a constant value. For either the three samples the constant value in the cubic regime is close to ~100 J/mol_O·K.

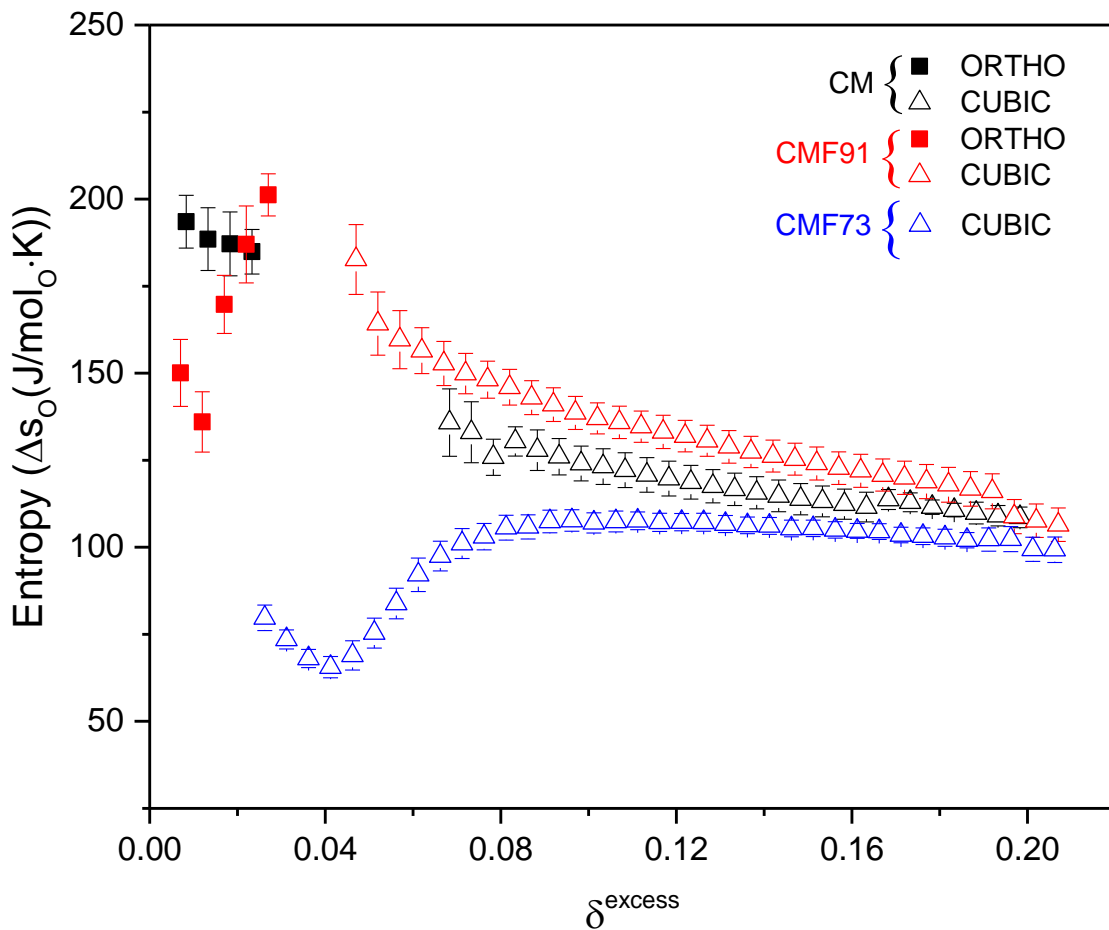
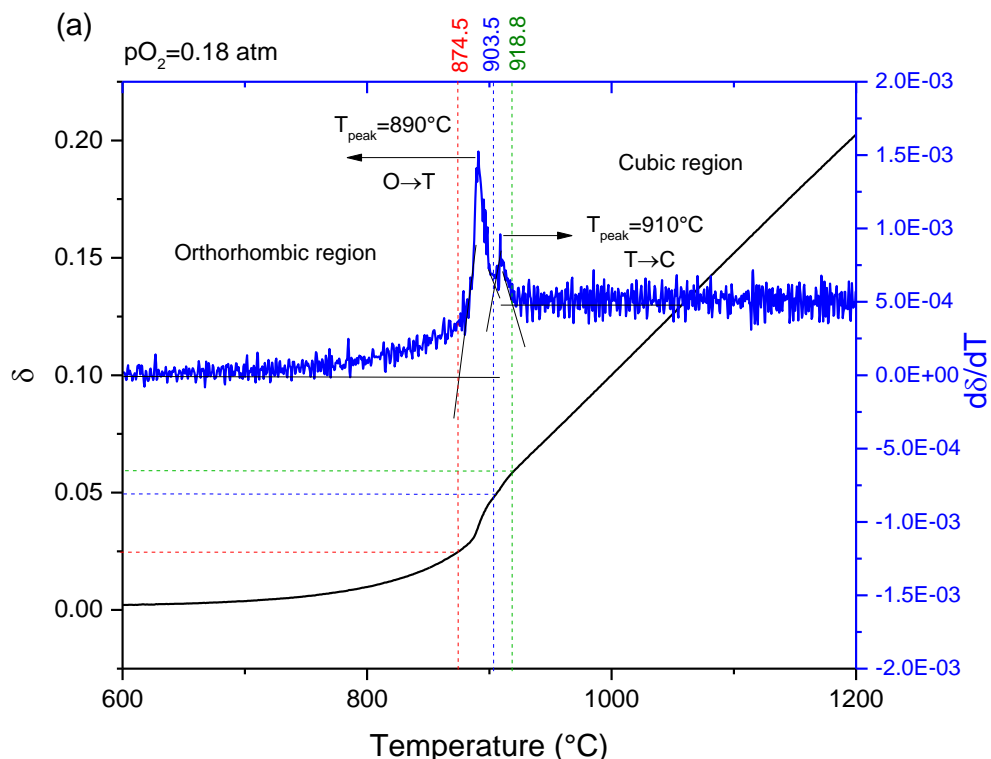


Figure A 11. Molar entropy (Δs_o (J/mol_O·K)) of CM, CMF91 and CMF73.

A.10 Procedure for the distinction of the (δ , T) points of the orthorhombic and cubic phase

Figure A 12 displays the $\delta(T)$ and $d\delta/dT$ profiles of CM samples under pO_2 of (a) 0.18 and (b) 0.008 atm. The (δ , T) points corresponding to the beginning and the end of the phase transitions have been identified. Taking into account that the phase transitions from orthorhombic to cubic structure is not iso-stoichiometric at the different pO_2 , hence the (δ , T) points corresponding to the cubic structure have been selected for temperatures progressively higher as the pO_2 decreases. The δ value corresponding to beginning of the phase transition has been taken in coincidence to the onset temperature of the first $d\delta/dT$ peak as exemplified in Figure A 12. Below that temperature the material is in the orthorhombic regime. While the δ value corresponding to the beginning of the cubic regime (end of the phase transition) has been taken in coincidence to the end of the first $d\delta/dT$ peak. In the temperature range under the $d\delta/dT$ peak the presence of the mixed orthorhombic/tetragonal/cubic phase prevent the correct extraction of the thermodynamic parameters. Hence, this temperature range has been excluded from the calculations. It is evident comparing Figure A 12a and b that at higher $pO_2=0.18$ atm (Figure A 12a) two $d\delta/dT$ peaks at 890 and 910 °C can be distinguished and respectively assigned to the orthorhombic to tetragonal phase transition ($O \rightarrow T$) and to the tetragonal to cubic one ($T \rightarrow C$), in agreement with DSC data. However, at lower $pO_2=0.008$ atm (Figure A 12b) only one peak can be distinguished. It is possible that, due to the lowering of the pO_2 , the phase transition $O \rightarrow T \rightarrow C$ could occur in a smaller temperature range thus making difficult to clearly distinguish each phase transition peak.



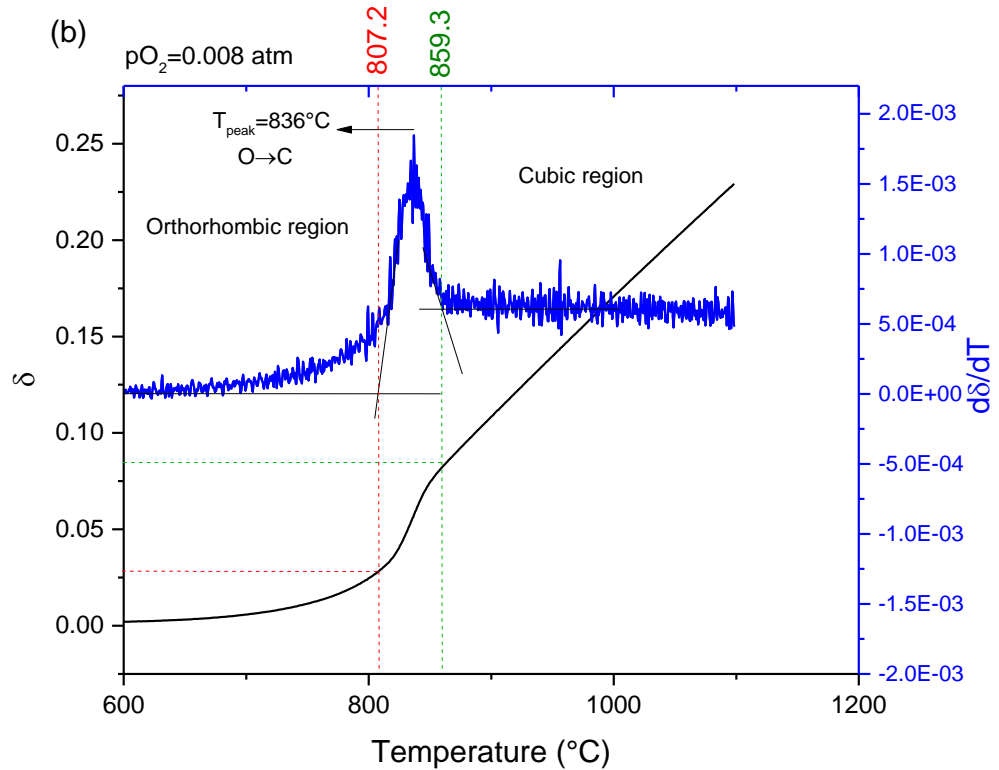


Figure A 12. δ and $d\delta/dT$ curves as a function of temperature of CM under pO_2 of (a) 0.18 and (b) 0.008 atm.

A.11 Heat storage capacity per unit mass of material (Q_M (kJ/kg_{ABO₃}))

The heat storage capacity per unit mass of material (Q_M (kJ/kg_{ABO₃})) plotted as a function of temperature at the different pO_2 investigated in this study for (a) CM, (b) CMF91 and (c) CMF73 is plotted in Figure A 13.

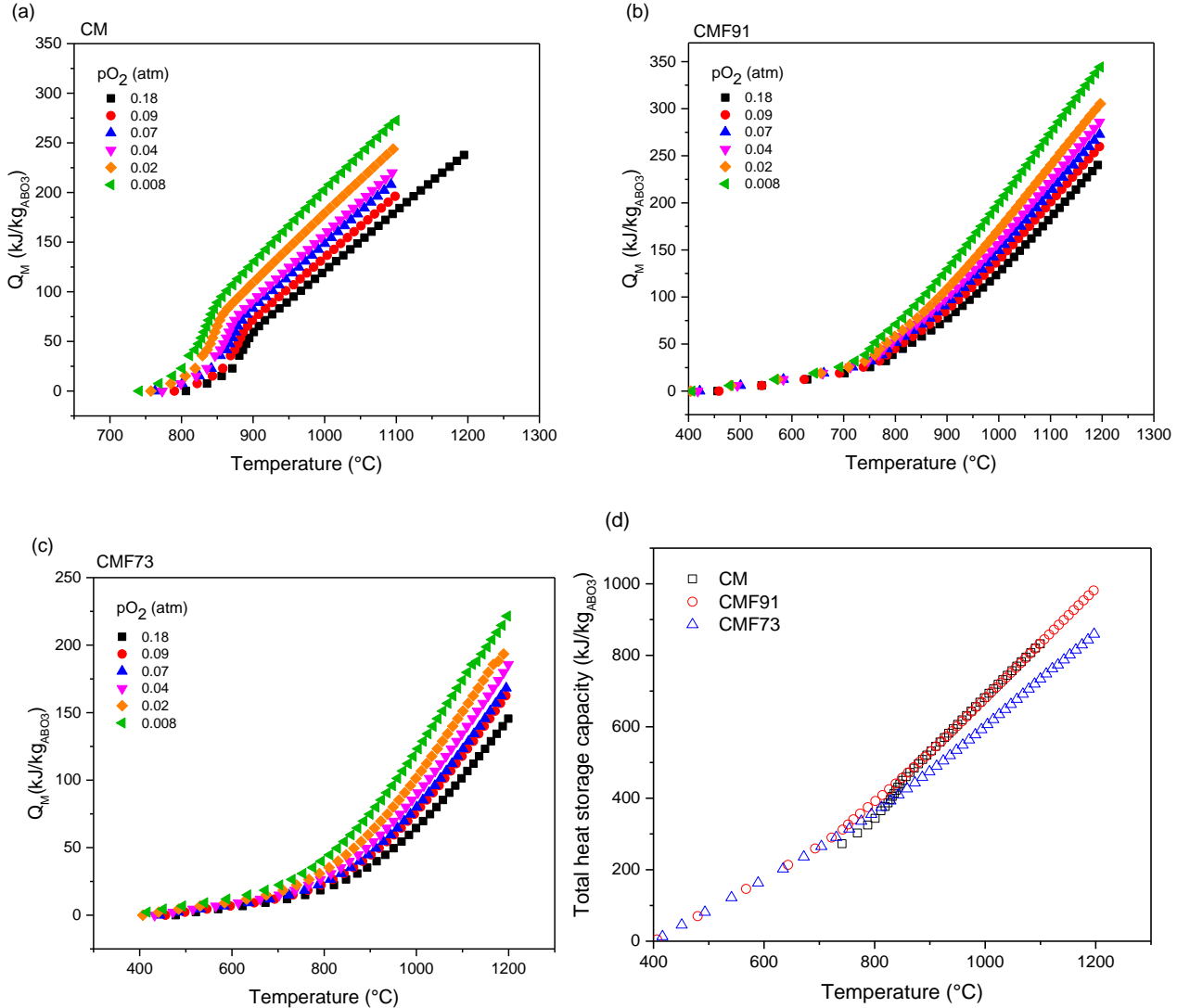


Figure A 13. Heat storage capacity per unit mass of material (Q_M (kJ/kg_{ABO₃})) plotted as a function of temperature at different pO_2 for (a) CM, (b) CMF91 and (c) CMF73. (d) Total heat storage capacity for CM, CMF91 and CMF73 calculated under a pO_2 of 0.008atm.